

Optimization of sources for focusing wave energy in targeted formations

This article has been downloaded from IOPscience. Please scroll down to see the full text article.

2010 J. Geophys. Eng. 7 242

(<http://iopscience.iop.org/1742-2140/7/3/003>)

View [the table of contents for this issue](#), or go to the [journal homepage](#) for more

Download details:

IP Address: 173.174.10.240

The article was downloaded on 09/06/2010 at 15:03

Please note that [terms and conditions apply](#).

Optimization of sources for focusing wave energy in targeted formations

C Jeong¹, L F Kallivokas^{1,3}, C Huh² and L W Lake²

¹ Department of Civil, Architectural and Environmental Engineering, The University of Texas at Austin, Austin, TX 78712, USA

² Department of Petroleum and Geosystems Engineering, The University of Texas at Austin, Austin, TX 78712, USA

E-mail: chanseok.jeong@gmail.com, loukas@mail.utexas.edu, chunhuh@mail.utexas.edu, larry.lake@mail.utexas.edu

Received 16 November 2009

Accepted for publication 20 April 2010

Published 9 June 2010

Online at stacks.iop.org/JGE/7/242

Abstract

We discuss a numerical approach for identifying the surface excitation that is necessary to maximize the response of a targeted subsurface formation. The motivation stems from observations in the aftermath of earthquakes, and from limited field experiments, whereby increased oil production rates were recorded and were solely attributable to the induced reservoir shaking. The observations suggest that focusing wave energy to the reservoir could serve as an effective low-cost enhanced oil recovery method. In this paper, we report on a general method that allows the determination of the source excitation, when provided with a desired maximization outcome at the targeted formation. We discuss, for example, how to construct the excitation that will maximize the kinetic energy in the target zone, while keeping silent the neighbouring zones. To this end, we cast the problem as an inverse-source problem, and use a partial-differential-equation-constrained optimization approach to arrive at an optimized source signal. We seek to satisfy stationarity of an augmented functional, which formally leads to a triplet of state, adjoint and control problems. We use finite elements to resolve the state and adjoint problems, and an iterative scheme to satisfy the control problem to converge to the sought source signal. We report on one-dimensional numerical experiments in the time domain involving a layered medium of semi-infinite extent. The numerical results show that the targeted formation's kinetic energy resulting from an optimized wave source could be several times greater than the one resulting from a blind source choice, and could overcome the mobility threshold of entrapped reservoir oil.

Keywords: elastic waves, inverse problems, EOR

(Some figures in this article are in colour only in the electronic version)

1. Introduction

During a typical crude oil production process, only 30–50% of the original-oil-in-place (OOIP) can be produced by a combination of the primary oil recovery mode (a reservoir's natural pressure) and water-flooding—the most widely used secondary recovery mode. To recover any oil still remaining in an existing reservoir, enhanced oil recovery (EOR) methods, such as gas- and polymer-flooding, should be employed

(Lake 1989). By and large, and beyond site-specific technical reasons that are of importance, the choice of a specific EOR method is driven chiefly by economic considerations. Low-cost and reliable EOR methods are thus of significance for the exploitation of any remaining reservoir capacity.

The so-called seismic- or wave-based EOR methods offer such a low-cost alternative, provided they can be shown to effectively mobilize oil. The key premise of wave-based EOR methods hinges on the ability of surficial wave sources to deliver sufficient vibrational energy to an existing reservoir to induce oil mobility.

³ Author to whom any correspondence should be addressed.

Several field observations seem to support the central macroscopic hypothesis that reservoir shaking, however it may be triggered, may lead to increased oil production. For example, increased rates have been reported in the aftermath of earthquakes (Steinbrugge and Moran 1954, Smimova 1968, Voytov *et al* 1972, Osika 1981), which were subsequently sustained for a few days after the main seismic event, without necessarily the presence/help of strong aftershocks. Similarly, in field applications of wave-based EOR in active or believed-as-depleted oil fields, where the vibrations were induced by either ground-surface or borehole wave sources, increased production rates have also been reported (Kuznetsov and Nikolaev 1990, Kouznetsov *et al* 1998, Westermarck *et al* 2001, Kuznetsov *et al* 2002, Guo *et al* 2004, Zhu and Xutao 2005).

Even though there appears to be a clear link between the induced shaking and production increases, research in the precise generative mechanisms that lead to increased oil mobility is rather thin. Beresnev's work (Beresnev and Johnson 1994, Iassonov and Beresnev 2003, Beresnev 2006) is among the very few where attempts have been made to bridge the scales between the reservoir's exposure to wave energy and an individual oil droplet's mobility. In Beresnev and Johnson (1994), Beresnev suggested the loss or reduction of an oil droplets adherence to the pore-surface wall, because of the wall's oscillation, as the predominant mechanism for increased mobility. To investigate the effect the waves have on the motion of an oil droplet entrapped in the pore space, Iassonov and Beresnev (2003) built a threshold capillary-trapping model of an oil droplet in a porous medium, and subjected it to low-frequency vibration. Subsequent experimental investigations (Li *et al* 2005), and numerical simulations (Beresnev 2006), indicated that a sufficiently large acceleration of the pore-surface wall must be induced, at least of the order of $1\text{--}10\text{ m s}^{-2}$, to mobilize the oil droplet in the pore space by the vibrating pore-surface walls. However, Beresnev also indicated that very low accelerations ($<0.1\text{ m s}^{-2}$) may be sufficient for mobilizing significant oil volumes, depending on the ganglion colony's mobility threshold.

It has also been argued (Surguchev *et al* 2002, Huh 2006) that reservoir shaking could lead to cross-flow in a fractured reservoir between the low- and high-permeability areas. Elastic waves induce differential pore pressure between layers of different permeability, and thus, the resulting pressure gradient between the two areas could lead to cross-flow, which, then, effectively mobilizes the bypassed oil from the low- to the high-permeability area (figure 1).

Whether wave energy could result in acceleration fields capable of overcoming the mobility threshold of oil droplets in thoroughly water-flooded reservoir regions, or could induce cross-flow owing to the development of strong pressure gradients, it is possible to sketch, given a specific goal for the reservoir region, an approach that would maximize the sought outcome. For example, if EOR were to be facilitated by maximizing the acceleration field in a target reservoir, or by maximizing the reservoir's kinetic energy or by maximizing the pressure gradients between the low- and high-permeability zones (assumed to be known), then an unconstrained optimization problem can be cast such that,

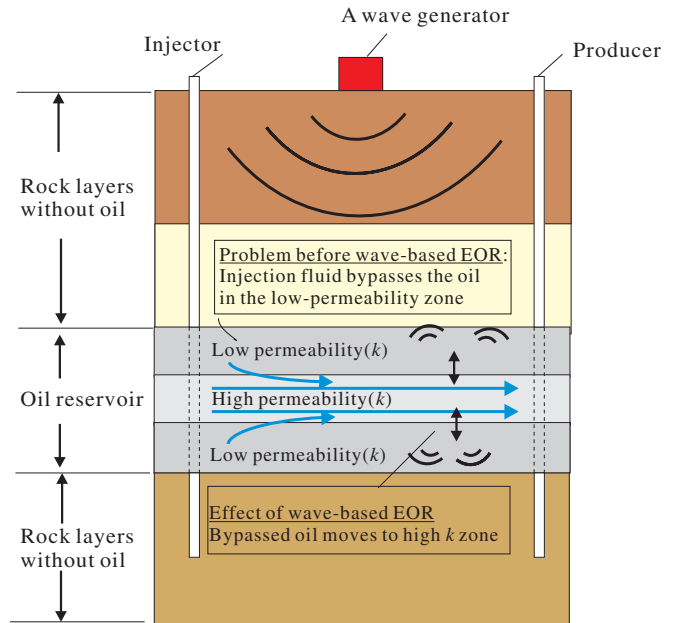


Figure 1. Possible outcome of a seismic wave-based EOR method.

upon solution, the necessary input excitations to optimally achieve the sought outcome would be obtained.

In this paper, we describe such an approach, whereby we seek to identify the unknown ground-surface load that could maximize the kinetic energy of a targeted formation within a heterogeneous domain. The problem, as described, leads formally to an inverse-source problem where the domain's properties and geometry are known, the response (or some measure thereof) ought to be maximized and the source load to achieve the response maximization is unknown. We adopt a partial-differential-equation-constrained optimization scheme to resolve and completely define the unknown source. We start with an objective functional, and augment it with the side imposition of the governing equations reflecting the physics of the wave propagation in the heterogeneous formation. We then seek to satisfy the first-order optimality conditions that formally lead to a triplet of state, adjoint and control problems, which, in turn, allow for the determination of the source. We use a prototype one-dimensional problem to describe the method.

From the onset we remark that the one-dimensional problem is overly simplistic in at least two ways: firstly, one-dimensional excitation conditions are impossible to replicate in practice. Secondly, the undamped one-dimensional model we adopt here ignores all of the three attenuation mechanisms typically associated with the passage of waves in the Earth: radiation attenuation due to an expanding wavefront, intrinsic attenuation due to wave energy conversion to heat and apparent attenuation due to scattering effects. As a result, the energy demand to attain in practice what one-dimensional analysis would predict is, in general, underestimated. Nevertheless, our discussion aims at highlighting the method's potential as a tool for prescribing ground sources, with the selective shaking of a targeted formation in mind. At the end, the numerical results, even under the one-dimensional simplifying

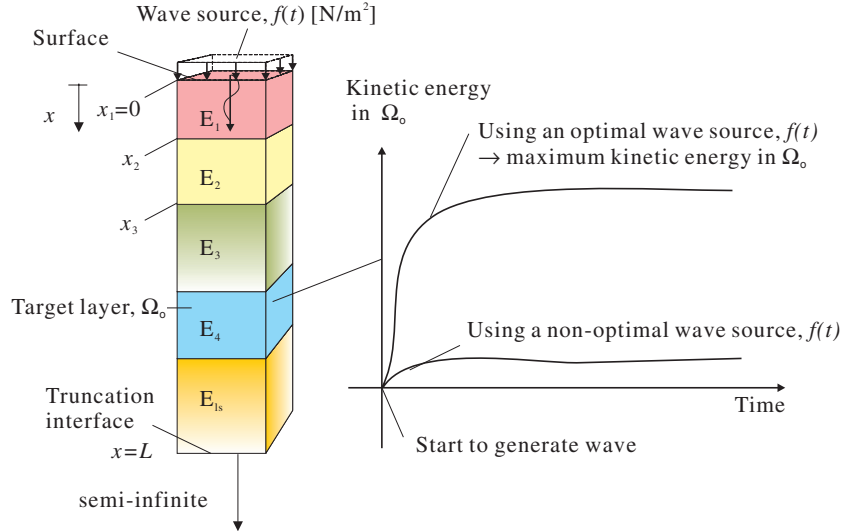


Figure 2. Schematic of inverse-source problem: a layered semi-infinite medium truncated at depth $x = L$, subjected to an unknown surface excitation. Ω_0 denotes the target layer. The right graph is the sought outcome: the maximization of Ω_0 's kinetic energy.

assumption, seem to be promising for the more realistic three-dimensional problem.

2. Problem definition

A semi-infinite heterogeneous (layered) medium is subjected to an excitation on the surface ($x = 0$) whose temporal variability $f(t)$ is unknown. We seek to identify $f(t)$ such that the kinetic energy within a target region (layer) Ω_0 is maximized (figure 2). The semi-infinite extent of the original domain is truncated through the introduction of a truncation boundary at some depth $x = L$. The propagation of compressional elastic waves within the truncated layered medium ($\Omega = (0, L)$) can be described by the following initial and boundary value problem (IBVP): we find the one-dimensional displacement field $u \equiv u(x, t)$ such that

$$\frac{\partial}{\partial x} \left(E(x) \frac{\partial u(x, t)}{\partial x} \right) - \rho(x) \frac{\partial^2 u(x, t)}{\partial t^2} = 0, \quad x \in (0, L), \quad t \in (0, T], \quad (1a)$$

$$E(0) \frac{\partial u}{\partial x}(0, t) + f(t) = 0, \quad t \in (0, T], \quad (1b)$$

$$\frac{\partial u}{\partial x}(L, t) + \frac{1}{c(L)} \frac{\partial u}{\partial t}(L, t) = 0, \quad t \in (0, T], \quad (1c)$$

$$u(x, 0) = 0, \quad x \in (0, L), \quad (1d)$$

$$\frac{\partial u}{\partial t}(x, 0) = 0, \quad x \in (0, L), \quad (1e)$$

where x denotes the location, t denotes the time; T denotes the total observation time, E represents the modulus⁴, ρ represents the density and $c = \sqrt{E/\rho}$ is the wave propagation speed. Condition (1b) is the surface excitation condition; (1c) is the truncation interface condition, which is exact for homogeneous domains, but only approximate for heterogeneous domains,

⁴ For example, for compressional waves $E = \lambda + 2\mu$, where λ and μ are the Lamé constants.

and (1d) and (1e) indicate that the system is initially at rest. Equation (1a) accounts, in general, for arbitrary heterogeneity (i.e. $E \equiv E(x)$); though the approach we follow applies to arbitrarily heterogeneous domains, we restrict the presentation, and the numerical results, to layered domains, comprising N_{ls} layers. In such a case, (1a) holds within each layer, and E_i refers to the resident i th layer modulus; in addition, the following interface conditions must hold:

$$E_i \left[\frac{\partial u}{\partial x} \right]_{x=x_{i+1}^-} = E_{i+1} \left[\frac{\partial u}{\partial x} \right]_{x=x_{i+1}^+}, \quad i = 1, \dots, (N_{ls} - 1), \quad (2a)$$

$$u|_{x=x_{i+1}^-} = u|_{x=x_{i+1}^+}, \quad i = 1, \dots, (N_{ls} - 1), \quad (2b)$$

where (2a) and (2b) are the traction and displacement interface continuity conditions, respectively. If the excitation $f(t)$ were known, the IBVP (1) can be solved to obtain the medium's response $u(x, t)$. The excitation, however, is unknown: to estimate it, we minimize the following functional:

$$\mathcal{L} = \frac{1}{\int_{\Omega_0} \int_0^T \rho(x) \left[\frac{\partial u}{\partial t}(x, t) \right]^2 dt dx}, \quad (3)$$

which involves the reciprocal of the target layer's kinetic energy⁵, evaluated over the entire observation time. We remark that (3) is only one of various candidate functionals that could be cast with the goal of maximizing oil droplet mobility in a targeted zone (e.g. maximizing the acceleration field). Numerically, we have experimented with (3) as well as the following functional:

$$\mathcal{L} = \frac{\int_{\Omega \setminus \Omega_0} \int_0^T \rho(x) \left[\frac{\partial u}{\partial t}(x, t) \right]^2 dt dx}{\int_{\Omega_0} \int_0^T \rho(x) \left[\frac{\partial u}{\partial t}(x, t) \right]^2 dt dx}, \quad (4)$$

which aims at maximizing the target's kinetic energy (Ω_0), while keeping the neighbouring layers ($\Omega \setminus \Omega_0$) as dormant as

⁵ We omit the usual $\frac{1}{2}$ term implicated in the kinetic energy's definition from the denominator of (3), since it does not affect the subsequent optimization process.

possible. The minimization of either (3) or (4) is tantamount to a constrained optimization problem owing to its subjugation to the governing IBVP. From a wave propagation point of view, we note that the IBVP (1) models compressional waves only: this is a consequence of considering the one-dimensional prototype, but is in no way a limitation of the described approach.

3. The inverse-source problem

To recast the constrained optimization problem into an unconstrained problem, we side-impose via Lagrange multipliers (or adjoint variables) the governing IBVP to either of the two minimization functionals (3) or (4). The governing IBVP involves the unknown excitation, parameterized using a finite set of parameters. The process must yield the optimal excitation parameters.

There arises an augmented functional, for which we seek a stationary point by enforcing the vanishing of first-order optimality conditions. Three optimality conditions are necessary: the first results from the variation of the augmented functional with respect to the Lagrange multipliers. As will be shown, the resulting form is simply the original IBVP or state problem. The variation with respect to the state variable, u , will lead to an adjoint problem for the Lagrange multipliers, which is a final value boundary value problem (FBVP). Lastly, it is the third problem—the control problem—arising from variations with respect to the excitation parameters that will allow the iterative update of the excitation parameters until convergence.

3.1. Augmented functional

The side imposition of the governing partial-differential equation (1a), and the associated boundary and initial conditions, (1b)–(1e), to the objective functional (3) via Lagrange multipliers λ , λ_0 , λ_L , λ_u and λ_v yields the augmented functional \mathcal{A} :

$$\begin{aligned} \mathcal{A} = & \left\{ \left(\frac{1}{\int_{\Omega_0} \int_0^T \rho \left[\frac{\partial u}{\partial t} \right]^2 dt dx} \right) + \int_0^L \int_0^T \lambda(x, t) \right. \\ & \times \left[\frac{\partial}{\partial x} \left(E(x) \frac{\partial u(x, t)}{\partial x} \right) - \rho \frac{\partial^2 u(x, t)}{\partial t^2} \right] dt dx \\ & + \int_0^T \lambda_0(t) \left[E(0) \frac{\partial u}{\partial x}(0, t) + f(t) \right] dt \\ & + \int_0^T \lambda_L(t) E(L) \left[\frac{\partial u}{\partial x}(L, t) + \frac{1}{c} \frac{\partial u}{\partial t}(L, t) \right] dt \\ & + \int_0^L \lambda_u(x) \left[\frac{\rho}{T} u(x, 0) \right] dx \\ & \left. + \int_0^L \lambda_v(x) \left[\rho \frac{\partial u}{\partial t}(x, 0) \right] dx \right\}, \end{aligned} \quad (5)$$

where the notation of the Lagrange multiplier differs depending on the side constraint: $\lambda(x, t)$, $\lambda_0(t)$, $\lambda_L(t)$, $\lambda_u(x)$ and $\lambda_v(x)$ denote the Lagrange multipliers for imposing the governing PDE (1a), the Neumann boundary condition

(1b), the truncation boundary condition (1c) and the initial conditions (1d) and (1e), respectively, in the augmented functional (5). Nevertheless, the dimensions of the Lagrange multipliers are identical to each other. As will be shown, $\lambda(x, t)$ can absorb the other Lagrange multipliers such that the ensuing adjoint problem is constructed solely in terms of $\lambda(x, t)$.

3.2. The first-order optimality conditions

Next, we enforce the vanishing of the first variations of the augmented functional \mathcal{A} with respect to the state variable (u), the adjoint variables (λ , λ_0 , λ_L , λ_u and λ_v) and a metric ξ expressing the parameterization of the unknown excitation $f(t)$. As will be shown,

$$\begin{cases} \delta_\lambda \mathcal{A} = 0 \\ \delta_{\lambda_0} \mathcal{A} = 0 \\ \delta_{\lambda_L} \mathcal{A} = 0 \\ \delta_{\lambda_u} \mathcal{A} = 0 \\ \delta_{\lambda_v} \mathcal{A} = 0 \end{cases} \quad \text{yields the state IBV problem,}$$

$$\delta_u \mathcal{A} = 0 \quad \text{yields the adjoint FBV problem,}$$

$$\delta_\xi \mathcal{A} = 0 \quad \text{yields the control problem.}$$

3.2.1. The first condition. The variation of \mathcal{A} with respect to λ , λ_0 , λ_L , λ_u and λ_v yields, respectively (henceforth, we drop the functional dependence for brevity wherever there is no ambiguity),

$$\delta_\lambda \mathcal{A} = \int_0^L \int_0^T \delta \lambda \left[\frac{\partial}{\partial x} \left(E \frac{\partial u}{\partial x} \right) - \rho \frac{\partial^2 u}{\partial t^2} \right] dt dx = 0, \quad (6a)$$

$$\delta_{\lambda_0} \mathcal{A} = \int_0^T \delta \lambda_0 \left[E \frac{\partial u}{\partial x} + f(t) \right] dt \Big|_{x=0} = 0, \quad (6b)$$

$$\delta_{\lambda_L} \mathcal{A} = \int_0^T \delta \lambda_L \left[E \frac{\partial u}{\partial x} + \frac{E}{c} \frac{\partial u}{\partial t} \right] dt \Big|_{x=L} = 0, \quad (6c)$$

$$\delta_{\lambda_u} \mathcal{A} = \int_0^L \delta \lambda_u \left[\frac{\rho}{T} u \right] dx \Big|_{t=0} = 0, \quad (6d)$$

$$\delta_{\lambda_v} \mathcal{A} = \int_0^L \delta \lambda_v \left[\rho \frac{\partial u}{\partial t} \right] dx \Big|_{t=0} = 0. \quad (6e)$$

For (6) to vanish for arbitrary $\delta \lambda$, $\delta \lambda_0$, $\delta \lambda_L$, $\delta \lambda_u$ and $\delta \lambda_v$, the following state problem must be satisfied:

$$\frac{\partial}{\partial x} \left(E \frac{\partial u}{\partial x} \right) - \rho \frac{\partial^2 u}{\partial t^2} = 0, \quad x \in (0, L), \quad t \in (0, T], \quad (7a)$$

$$E(0) \frac{\partial u}{\partial x}(0, t) + f(t) = 0, \quad t \in (0, T], \quad (7b)$$

$$\frac{\partial u}{\partial x}(L, t) + \frac{1}{c} \frac{\partial u}{\partial t}(L, t) = 0, \quad t \in (0, T], \quad (7c)$$

$$u(x, 0) = 0, \quad x \in (0, L), \quad (7d)$$

$$\frac{\partial u}{\partial t}(x, 0) = 0, \quad x \in (0, L). \quad (7e)$$

As can be seen, the resulting state problem is identical to the IBVP (1). We remark that, in the layered case, (7a) is written for every layer, and that the interface continuity conditions are formally recoverable; we will illustrate the layered case with the adjoint problem.

3.2.2. *The second condition.* The vanishing of the variation of the augmented functional \mathcal{A} with respect to the state variable u yields

$$\begin{aligned} \delta_u \mathcal{A} = & \delta_u \left[\left(\frac{1}{\int_{\Omega_0} \int_0^T \rho \left[\frac{\partial u}{\partial t} \right]^2 dt dx} \right) \right. \\ & + \int_0^L \int_0^T \lambda \left[\frac{\partial}{\partial x} \left(E \frac{\partial u}{\partial x} \right) - \rho \frac{\partial^2 u}{\partial t^2} \right] dt dx \\ & + \int_0^T \lambda_0 \left[E \frac{\partial u}{\partial x} + f(t) \right] dt \Big|_{x=0} \\ & + \int_0^T \lambda_L \left[E \frac{\partial u}{\partial x} + \frac{E}{c} \frac{\partial u}{\partial t} \right] dt \Big|_{x=L} \\ & \left. + \int_0^L \lambda_u \left[\frac{\rho}{T} u \right] dx \Big|_{t=0} + \int_0^L \lambda_v \left[\rho \frac{\partial u}{\partial t} \right] dx \Big|_{t=0} \right] = 0. \quad (8) \end{aligned}$$

Applying the variation, taking into account that δu and $\frac{\partial \delta u}{\partial t}$ vanish at $t = 0$, and after operating on the first term, (8) reduces to

$$\begin{aligned} \delta_u \mathcal{A} = & - \frac{2 \left[\int_{\Omega_0} \rho \left[\frac{\partial u}{\partial t} \delta u \right] dx \Big|_{t=T} - \int_{\Omega_0} \int_0^T \rho \left[\frac{\partial^2 u}{\partial t^2} \delta u \right] dt dx \right]}{\left(\int_{\Omega_0} \int_0^T \rho \left[\frac{\partial u}{\partial t} \right]^2 dt dx \right)^2} \\ & + \int_0^L \int_0^T \lambda \left[\frac{\partial}{\partial x} \left(E \frac{\partial \delta u}{\partial x} \right) - \rho \frac{\partial^2 \delta u}{\partial t^2} \right] dt dx \\ & + \int_0^T \lambda_0 \left[E \frac{\partial \delta u}{\partial x} \right] dt \Big|_{x=0} \\ & + \int_0^T \lambda_L \left[E \frac{\partial \delta u}{\partial x} + \frac{E}{c} \frac{\partial \delta u}{\partial t} \right] dt \Big|_{x=L} = 0. \quad (9) \end{aligned}$$

Next, we isolate the second term whose first component becomes (for a layered medium case)

$$\begin{aligned} & \int_0^L \int_0^T \left[\lambda \frac{\partial}{\partial x} \left(E \frac{\partial \delta u}{\partial x} \right) \right] dt dx \\ & = \int_0^L \int_0^T \left[\lambda \frac{\partial E}{\partial x} \frac{\partial \delta u}{\partial x} + \lambda E \frac{\partial^2 \delta u}{\partial x^2} \right] dt dx \\ & = \sum_{i=1}^{N_{\text{ls}}} \left\{ \int_{x_i^+}^{x_{i+1}^-} \int_0^T \left[\lambda \frac{\partial E_i}{\partial x} \frac{\partial \delta u}{\partial x} + \lambda E_i \frac{\partial^2 \delta u}{\partial x^2} \right] dt dx \right\} \\ & = \sum_{i=1}^{N_{\text{ls}}} \left\{ \left[\int_0^T \lambda \frac{\partial E_i}{\partial x} \delta u dt \right]_{x_i^+}^{x_{i+1}^-} \right. \\ & \quad - \int_{x_i^+}^{x_{i+1}^-} \int_0^T \left[\frac{\partial}{\partial x} \left(\lambda \frac{\partial E_i}{\partial x} \right) \delta u \right] dt dx \\ & \quad + \left[\int_0^T \lambda E_i \frac{\partial \delta u}{\partial x} dt \right]_{x_i^+}^{x_{i+1}^-} \\ & \quad \left. - \int_{x_i^+}^{x_{i+1}^-} \int_0^T \left[\frac{\partial}{\partial x} (\lambda E_i) \frac{\partial \delta u}{\partial x} \right] dt dx \right\}. \quad (10) \end{aligned}$$

Equation (10) can be rearranged to yield

$$\begin{aligned} & \int_0^L \int_0^T \left[\lambda \frac{\partial}{\partial x} \left(E \frac{\partial \delta u}{\partial x} \right) \right] dt dx \\ & = \sum_{i=1}^{N_{\text{ls}}-1} \left\{ \left[\int_0^T \lambda E_i \frac{\partial \delta u}{\partial x} dt \right]_{x=x_{i+1}^-} - \left[\int_0^T \lambda E_{i+1} \frac{\partial \delta u}{\partial x} dt \right]_{x=x_i^+} \right\} \end{aligned}$$

$$\begin{aligned} & - \left[\int_0^T \left(E_i \frac{\partial \lambda}{\partial x} \right) \delta u dt \right]_{x=x_{i+1}^-} \\ & + \left[\int_0^T \left(E_{i+1} \frac{\partial \lambda}{\partial x} \right) \delta u dt \right]_{x=x_i^+} \Big\} \\ & - \left[\int_0^T \lambda E \frac{\partial \delta u}{\partial x} dt \right]_{x=0} + \left[\int_0^T \lambda E \frac{\partial \delta u}{\partial x} dt \right]_{x=L} \\ & + \left[\int_0^T \left(E \frac{\partial \lambda}{\partial x} \right) \delta u dt \right]_{x=0} - \left[\int_0^T \left(E \frac{\partial \lambda}{\partial x} \right) \delta u dt \right]_{x=L} \\ & + \int_0^L \int_0^T \left[\frac{\partial}{\partial x} \left(\frac{\partial \lambda}{\partial x} E \right) \right] \delta u dt dx. \quad (11) \end{aligned}$$

Next, the second component of the second term in (9), after integration by parts with respect to time, leads to the following:

$$\begin{aligned} & \int_0^L \int_0^T \left[\lambda \rho \frac{\partial^2 \delta u}{\partial t^2} \right] dt dx \\ & = \int_0^L \left[\rho \lambda \frac{\partial \delta u}{\partial t} \right] dx \Big|_{t=T} - \int_0^L \left[\rho \frac{\partial \lambda}{\partial t} \delta u \right] dx \Big|_{t=T} \\ & \quad + \int_0^L \int_0^T \left[\rho \frac{\partial^2 \lambda}{\partial t^2} \delta u \right] dt dx. \quad (12) \end{aligned}$$

In addition,

$$\begin{aligned} & \int_0^T \left[\lambda_L \frac{E}{c} \frac{\partial \delta u}{\partial t} \right] dt \Big|_{x=L} \\ & = \left[\lambda_L \frac{E}{c} \delta u \right]_{x=L, t=T} - \int_0^T \left[\frac{\partial \lambda_L}{\partial t} \frac{E}{c} \right] \delta u dt \Big|_{x=L}. \quad (13) \end{aligned}$$

Then, by combining (11), (12) and (13), (9) can be rearranged as

$$\begin{aligned} \delta_u \mathcal{A} = & \int_0^L \int_0^T \delta u \left[\frac{\partial}{\partial x} \left(\frac{\partial \lambda}{\partial x} E \right) - \rho \frac{\partial^2 \lambda}{\partial t^2} + \mathcal{E}(x) \rho \frac{\partial^2 u}{\partial t^2} \right] dt dx \\ & + \int_0^L \delta u \left[\rho \frac{\partial \lambda}{\partial t} - \mathcal{E}(x) \rho \frac{\partial u}{\partial t} \right] dx \Big|_{t=T} \\ & - \int_0^L \left[\rho \lambda \frac{\partial \delta u}{\partial t} \right] dx \Big|_{t=T} + \left[\lambda_L \frac{E}{c} \delta u \right]_{x=L, t=T} \\ & - \int_0^T \left[\lambda E \frac{\partial \delta u}{\partial x} \right] dt \Big|_{x=0} + \int_0^T \left[\lambda_0 E \frac{\partial \delta u}{\partial x} \right] dt \Big|_{x=0} \\ & + \int_0^T \left[\lambda E \frac{\partial \delta u}{\partial x} \right] dt \Big|_{x=L} + \int_0^T \left[\lambda_L E \frac{\partial \delta u}{\partial x} \right] dt \Big|_{x=L} \\ & + \int_0^T \left[E \frac{\partial \lambda}{\partial x} \delta u \right] dt \Big|_{x=0} - \int_0^T \left[\frac{\partial \lambda_L}{\partial t} \frac{E}{c} + E \frac{\partial \lambda}{\partial x} \right] \delta u dt \Big|_{x=L} \\ & + \sum_{i=1}^{N_{\text{ls}}-1} \left\{ \left[\int_0^T \lambda E_i \frac{\partial \delta u}{\partial x} dt \right]_{x=x_{i+1}^-} \right. \\ & \quad - \left[\int_0^T \lambda E_{i+1} \frac{\partial \delta u}{\partial x} dt \right]_{x=x_i^+} - \left[\int_0^T E_i \frac{\partial \lambda}{\partial x} \delta u dt \right]_{x=x_{i+1}^-} \\ & \quad \left. + \left[\int_0^T E_{i+1} \frac{\partial \lambda}{\partial x} \delta u dt \right]_{x=x_i^+} \right\} = 0, \quad (14) \end{aligned}$$

where

$$\mathcal{E}(x) = \begin{cases} \frac{2}{\left(\int_{\Omega_0} \int_0^T \rho \left[\frac{\partial u(x,t)}{\partial t} \right]^2 dt dx \right)^2}, & x \in \Omega_0 \\ 0, & x \in \Omega \setminus \Omega_0. \end{cases} \quad (15)$$

For (14) to be satisfied for arbitrary δu , we require the satisfaction of the following *adjoint problem*:

$$\frac{\partial}{\partial x} \left(E \frac{\partial \lambda}{\partial x} \right) - \rho \frac{\partial^2 \lambda}{\partial t^2} = -\mathcal{E}(x) \rho \frac{\partial^2 u}{\partial t^2},$$

$$x \in (0, L), \quad t \in [0, T), \quad (16a)$$

$$\frac{\partial \lambda}{\partial x}(0, t) = 0, \quad t \in [0, T), \quad (16b)$$

$$\frac{\partial \lambda}{\partial x}(L, t) - \frac{1}{c(L)} \frac{\partial \lambda}{\partial t}(L, t) = 0, \quad t \in [0, T), \quad (16c)$$

$$\lambda(x, T) = 0, \quad x \in (0, L), \quad (16d)$$

$$\frac{\partial \lambda}{\partial t}(x, T) = \mathcal{E}(x) \frac{\partial u}{\partial t}(x, T), \quad x \in (0, L), \quad (16e)$$

with the continuity conditions

$$\lambda|_{x=x_{i+1}^-} = \lambda|_{x=x_{i+1}^+}, \quad (17a)$$

$$E_i \left[\frac{\partial \lambda}{\partial x} \right]_{x=x_{i+1}^-} = E_{i+1} \left[\frac{\partial \lambda}{\partial x} \right]_{x=x_{i+1}^+}, \quad (17b)$$

and

$$\lambda_L(t) = -\lambda(L, t), \quad (17c)$$

$$\lambda_0(t) = \lambda(0, t). \quad (17d)$$

The adjoint problem has structure identical to the state problem, except for the following differences: whereas the state problem is driven by the excitation term in the surface condition (7b), the adjoint problem is driven by body forces localized to the target layer and expressed in terms of the accelerations of the state problem (per (16a)). Secondly, as can be seen from (16d) and (16e), the adjoint problem is a final value BVP; thirdly, the sign of the time derivative in the truncation condition (16c) has been changed when compared with the truncation condition of the state problem (7c), owing to the reversal of the time line in the adjoint problem.

The preceding development was based upon using (3) as the objective functional. If, to force the neighbouring layers to be silent, we choose (4), the resulting state and adjoint problems remain the same as derived above, provided the definition of $\mathcal{E}(x)$ is replaced by

$$\mathcal{E}(x) = \begin{cases} \frac{2 \int_{\Omega \setminus \Omega_0} \int_0^T \rho \left[\frac{\partial u(x,t)}{\partial t} \right]^2 dt dx}{\left(\int_{\Omega_0} \int_0^T \rho \left[\frac{\partial u(x,t)}{\partial t} \right]^2 dt dx \right)^2}, & x \in \Omega_0, \\ \frac{-2}{\left(\int_{\Omega_0} \int_0^T \rho \left[\frac{\partial u(x,t)}{\partial t} \right]^2 dt dx \right)}, & x \in \Omega \setminus \Omega_0. \end{cases} \quad (18)$$

3.2.3. The third condition. Next, we consider the variation of the augmented functional \mathcal{A} with respect to a scalar variable ξ , tantamount to parameter f_i —a nodal force of the discretized force function $f(t)$ (see (33)). To this end,

$$\delta_\xi \mathcal{A} = \frac{\partial}{\partial \xi} \left\{ \left(\frac{1}{\int_{\Omega_0} \int_0^T \rho \left[\frac{\partial u}{\partial t} \right]^2 dt dx} \right) + \int_0^L \int_0^T \lambda \left[\frac{\partial}{\partial x} \left(E \frac{\partial u}{\partial x} \right) - \rho \frac{\partial^2 u}{\partial t^2} \right] dt dx \right.$$

$$\left. + \int_0^T \lambda \left[E \frac{\partial u}{\partial x} + f(t) \right] dt \Big|_{x=0} - \int_0^T \lambda \left[E \frac{\partial u}{\partial x} + \frac{E}{c} \frac{\partial u}{\partial t} \right] dt \Big|_{x=L} + \int_0^L \lambda_u \left[\frac{\rho}{T} u \right] dx \Big|_{t=0} + \int_0^L \lambda_v \left[\rho \frac{\partial u}{\partial t} \right] dx \Big|_{t=0} \right\} = 0. \quad (19)$$

After some manipulation, (19) reduces to

$$\delta_\xi \mathcal{A} = - \int_0^L \int_0^T \left[E \frac{\partial \lambda}{\partial x} \frac{\partial \dot{u}}{\partial x} + \rho \lambda \frac{\partial^2 \dot{u}}{\partial t^2} + \mathcal{E}(x) \rho \frac{\partial u}{\partial t} \frac{\partial \dot{u}}{\partial t} \right] dt dx - \int_0^L \int_0^T \left[E \frac{\partial \dot{\lambda}}{\partial x} \frac{\partial u}{\partial x} + \rho \dot{\lambda} \frac{\partial^2 u}{\partial t^2} \right] dt dx + \int_0^T \left[\dot{\lambda} f(t) + \lambda \frac{\partial f(t)}{\partial \xi} \right] dt \Big|_{x=0} - \int_0^T \left[\dot{\lambda} \frac{E}{c} \frac{\partial u}{\partial t} + \lambda \frac{E}{c} \frac{\partial \dot{u}}{\partial t} \right] dt \Big|_{x=L} = 0, \quad (20)$$

where $(\dot{})$ denotes the derivative of the subtended function with respect to ξ . To further simplify (20), we introduce a weak form of the state problem using $\dot{\lambda}$ as the weight function to obtain

$$\int_0^L \int_0^T \dot{\lambda} \left\{ \frac{\partial}{\partial x} \left(E \frac{\partial u}{\partial x} \right) - \rho \frac{\partial^2 u}{\partial t^2} \right\} dt dx = 0. \quad (21)$$

After integration by parts, (21) becomes

$$\int_0^L \int_0^T \left[E \frac{\partial \dot{\lambda}}{\partial x} \frac{\partial u}{\partial x} + \dot{\lambda} \rho \frac{\partial^2 u}{\partial t^2} \right] dt dx = \left[\int_0^T \dot{\lambda} E \frac{\partial u}{\partial x} dt \right]_0^L. \quad (22)$$

Similarly, we introduce a weak form of the adjoint problem with \dot{u} as the weight function to obtain

$$\int_0^L \int_0^T \dot{u} \left\{ \frac{\partial}{\partial x} \left(\frac{\partial \lambda}{\partial x} E \right) - \rho \frac{\partial^2 \lambda}{\partial t^2} + \mathcal{E}(x) \rho \frac{\partial^2 u}{\partial t^2} \right\} dt dx = 0, \quad (23)$$

which after integration by parts leads to the following:

$$\int_0^L \int_0^T \left[\frac{\partial \dot{u}}{\partial x} \frac{\partial \lambda}{\partial x} E + \rho \frac{\partial^2 \dot{u}}{\partial t^2} \lambda + \frac{\partial \dot{u}}{\partial t} \mathcal{E}(x) \rho \frac{\partial u}{\partial t} \right] dt dx = \left[\int_0^T \dot{u} \frac{\partial \lambda}{\partial x} E dt \right]_{x=L}. \quad (24)$$

Because of (22) and (24), (20) simplifies to the following:

$$\delta_\xi \mathcal{A} = - \left[\int_0^T E \dot{\lambda} \frac{\partial u}{\partial x} dt \right]_{x=0}^{x=L} - \left[\int_0^T E \dot{u} \frac{\partial \lambda}{\partial x} dt \right]_{x=L} + \int_0^T \left[\dot{\lambda} f(t) + \lambda \frac{\partial f(t)}{\partial \xi} \right] dt \Big|_{x=0} - \int_0^T \left[\dot{\lambda} \frac{E}{c} \frac{\partial u}{\partial t} + \lambda \frac{E}{c} \frac{\partial \dot{u}}{\partial t} \right] dt \Big|_{x=L}. \quad (25)$$

There also holds

$$- \left[\int_0^T E \dot{\lambda} \frac{\partial u}{\partial x} dt \right]_{x=0}^{x=L} = \left[\int_0^T \dot{\lambda} \frac{E}{c} \frac{\partial u}{\partial t} dt \right]_{x=L} - \left[\int_0^T \dot{\lambda} f(t) dt \right]_{x=0}, \quad (26a)$$

$$-\int_0^T \left\{ \lambda \frac{E}{c} \frac{\partial \dot{u}}{\partial t} \right\} dt \Big|_{x=L} = \int_0^T \left\{ E \frac{\partial \lambda}{\partial x} \dot{u} \right\} dt \Big|_{x=L}, \quad (26b)$$

and thus, (25) reduces finally to the *control problem*

$$\delta_\xi \mathcal{A} (= \nabla_\xi \mathcal{A}) = \int_0^T \lambda \frac{\partial f(t)}{\partial \xi} dt \Big|_{x=0} = 0, \quad (27)$$

where λ , again, denotes the solution of the adjoint problem. We remark that $\delta_\xi \mathcal{A}$ is equivalent to the gradient of the objective functional $\nabla_\xi \mathcal{L}$, since the side-imposed constraints to the augmented functional \mathcal{A} vanish at the stationary point owing to the satisfaction of the state problem. To obtain the excitation parameters, we use a gradient-based minimization process and the control equation (27) as the reduced gradient. The details are given in the next section; if (4) were to be used instead of (3), the control problem remains unaltered.

4. Inverse problem solution and discrete forms

Satisfaction of the first-order optimality conditions, upon discretization, gives rise to a Karush–Kuhn–Tucker (KKT) system (Karush 1939, Kuhn and Tucker 1951). Stationarity can be achieved by solving the state, adjoint and control problems either as a fully coupled problem (a full-space solution approach) or via a reduced-space approach. Since the computational cost associated with a full-space approach is rather significant, we solve the KKT system by projecting the state and adjoint variables into the space of the control variables. Such a reduced-space solution approach entails the following steps: (a) first the state problem is solved for a trial form of the excitation; (b) the adjoint problem is then solved using as driver the acceleration field of the state problem (per (16a)); (c) finally, updates to the parameters defining the trial form of the excitation are obtained via a gradient-based scheme that uses the control equation (27) as the reduced gradient: at each iteration of the gradient-based scheme the control equation provides the search direction for the parameter updates.

4.1. State and adjoint semi-discrete forms

The first two steps entail the solution of both an IBVP (the state problem) and a FBVP (the adjoint problem). We use a classic Galerkin finite element approach to resolve the discrete state and adjoint problems. To this end, we multiply (1a) and (16a) by test functions, $w(x)$ and $v(x)$, respectively, and integrate by parts, to arrive at the following weak forms:

$$\int_0^L \left[E \frac{\partial w}{\partial x} \frac{\partial u}{\partial x} + \rho w \frac{\partial^2 u}{\partial t^2} \right] dx + \frac{E(L)}{c(L)} w(L) \frac{\partial u(L)}{\partial t} = w(0) f(t), \quad (28a)$$

$$\int_0^L \left[E \frac{\partial v}{\partial x} \frac{\partial \lambda}{\partial x} + \rho v \frac{\partial^2 \lambda}{\partial t^2} \right] dx - \frac{E(L)}{c(L)} v(L) \frac{\partial \lambda(L)}{\partial t} = \int_0^L \left[v \mathcal{E} \rho \frac{\partial^2 u}{\partial t^2} \right] dx. \quad (28b)$$

We introduce the following approximants:

$$w(x) = \mathbf{w}^T \mathbf{q}(x), \quad u(x) = \mathbf{q}^T(x) \mathbf{u}(t), \quad (29a)$$

$$v(x) = \mathbf{v}^T \mathbf{q}(x), \quad \lambda(x) = \mathbf{q}^T(x) \mathbf{z}(t), \quad (29b)$$

where $\mathbf{u}(t)$ and $\mathbf{z}(t)$ denote the vectors of the nodal solutions of $u(x, t)$ and $\lambda(x, t)$, respectively; \mathbf{w} and \mathbf{v} denote the vectors of the nodal quantities of the test functions, $w(x)$ and $v(x)$, respectively; and $\mathbf{q}(x)$ represents a vector of shape functions. Then, (28a) and (28b) are reduced into the following semi-discrete forms:

$$\mathbf{M} \frac{\partial^2 \mathbf{u}(t)}{\partial t^2} + \mathbf{C} \frac{\partial \mathbf{u}(t)}{\partial t} + \mathbf{K} \mathbf{u}(t) = \mathbf{F}(t), \quad (30a)$$

$$\mathbf{M} \frac{\partial^2 \mathbf{z}(t)}{\partial t^2} - \mathbf{C} \frac{\partial \mathbf{z}(t)}{\partial t} + \mathbf{K} \mathbf{z}(t) = \mathbf{P}(t), \quad (30b)$$

where

$$\mathbf{M} = \int_0^l [\rho(x) \mathbf{q}(x) \mathbf{q}^T(x)] dx, \quad (31a)$$

$$\mathbf{C} = \frac{E(L)}{c(L)} \mathbf{q}(L) \mathbf{q}^T(L), \quad (31b)$$

$$\mathbf{K} = \int_0^l \left[E(x) \frac{\partial \mathbf{q}(x)}{\partial x} \frac{\partial \mathbf{q}^T(x)}{\partial x} \right] dx, \quad (31c)$$

$$\mathbf{F}(t) = \mathbf{q}(0) f(t), \quad (31d)$$

$$\mathbf{P}(t) = \int_0^l [\mathcal{E} \rho \mathbf{q}(x) \mathbf{q}^T(x)] dx \frac{\partial^2 \mathbf{u}(t)}{\partial t^2}. \quad (31e)$$

We solve (30a) and (30b) using a Newmark time-integration scheme such that the state and adjoint solutions at each time step are obtained from the following linear system of equations:

$$\left[\mathbf{K} + \mathbf{C} \frac{2}{\Delta t} + \mathbf{M} \frac{4}{(\Delta t)^2} \right] \mathbf{u}_{(n+1)} = \mathbf{C} \left[\frac{2}{\Delta t} \mathbf{u}_{(n)} + \frac{\partial \mathbf{u}_{(n)}}{\partial t} \right] + \mathbf{M} \left[\frac{4 \mathbf{u}_{(n)}}{(\Delta t)^2} + \frac{4}{\Delta t} \frac{\partial \mathbf{u}_{(n)}}{\partial t} + \frac{\partial^2 \mathbf{u}_{(n)}}{\partial t^2} \right] + \mathbf{F}_{(n+1)}, \quad (32a)$$

$$\left[\mathbf{K} + \mathbf{C} \frac{2}{\Delta t} + \mathbf{M} \frac{4}{(\Delta t)^2} \right] \mathbf{z}_{(n)} = \mathbf{C} \left[\frac{2}{\Delta t} \mathbf{z}_{(n+1)} - \frac{\partial \mathbf{z}_{(n+1)}}{\partial t} \right] + \mathbf{M} \left[\frac{4 \mathbf{z}_{(n+1)}}{(\Delta t)^2} - \frac{4}{\Delta t} \frac{\partial \mathbf{z}_{(n+1)}}{\partial t} + \frac{\partial^2 \mathbf{z}_{(n+1)}}{\partial t^2} \right] + \mathbf{P}_{(n)}, \quad (32b)$$

where Δt denotes the time step, and the subscripts (n) and ($n+1$) denote evaluation of the nodal vectors at the n th and ($n+1$)st time steps. Note that the traversal of the time line in (32b) is reversed with respect to (32a). Moreover, reflecting the presence of similar operators in both the state and adjoint continuous problems, note that the matrices \mathbf{K} , \mathbf{C} and \mathbf{M} are shared by both discrete forms, requiring their formation only once per inversion iteration. We remark that there is only one system matrix inversion needed per (excitation) inversion iteration, owing to the fact that the left-hand sides of (32a) and (32b) are identical.

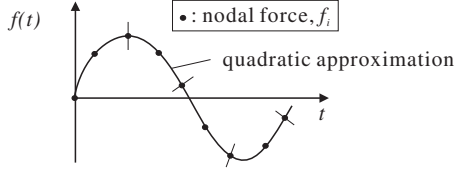


Figure 3. Schematic of parameterization of the unknown excitation $f(t)$ using quadratic shape functions.

4.2. Excitation temporal discretization

To compute the unknown time signal $f(t)$, we first parameterize it as (figure 3)

$$f(t) = \sum_{i=1}^{n_f} f_i \varphi_i(t), \quad (33)$$

where $\varphi_i(t)$ and f_i denote the i th shape function and nodal excitation parameter, respectively, and n_f is the total number of parameters. Following the temporal approximation of $f(t)$, the control equation (27) becomes

$$\delta_{\xi} \mathcal{A} = \int_0^T \lambda \frac{\partial f(t)}{\partial f_i} dt \Big|_{x=0} = \int_0^T \lambda \varphi_i(t) dt \Big|_{x=0} = 0. \quad (34)$$

We remark that the reduced gradient of the original functional \mathcal{L} can be cast as

$$\nabla_{f_i} \mathcal{L} = \int_0^T \lambda \varphi_i(t) dt \Big|_{x=0}, \quad (35)$$

which forms the basis for the parameter updates. The procedure is outlined next.

4.3. Excitation parameters updates

We perform a minimization process to arrive at a solution satisfying the first-order optimality conditions starting from $\mathbf{f}_{(0)}$ —the set of the initially guessed excitation parameters. At each iteration, we first solve the state problem using the excitation parameters obtained from the previous iteration; then, we solve the adjoint problem using the state solution; and finally, using the adjoint solutions, we compute the value of the gradient (35). Then, we update the excitation parameters as

$$\mathbf{f}_{(k+1)} = \mathbf{f}_{(k)} + \mathbf{g} \theta_{(k)}, \quad (36)$$

where $\mathbf{f}_{(k)}$ denotes the parameter vector at the k th iteration; $\theta_{(k)}$ denotes the step length for the k th iteration; \mathbf{g} denotes the search direction, which is obtained using (35) and a conjugate-gradient (CG) scheme (Fletcher and Reeves 1951, Nocedal and Wright 2006). We use the optimal value of $\theta_{(k)}$ such that sufficient decrease of the minimization functional is ensured at each iteration. That is, (a) if the sufficient decrease is not met, we use a backtracking method (Nocedal and Wright 2006)—reducing the step length by a factor of α until the sufficient decrease condition is satisfied; (b) after the excitation parameters are updated, we increase the step length at the next iteration by multiplying it by β to improve the rate of convergence. In the applications we used $\alpha = 0.9$ and $\beta = 1.1$. The entire algorithm is summarized below.

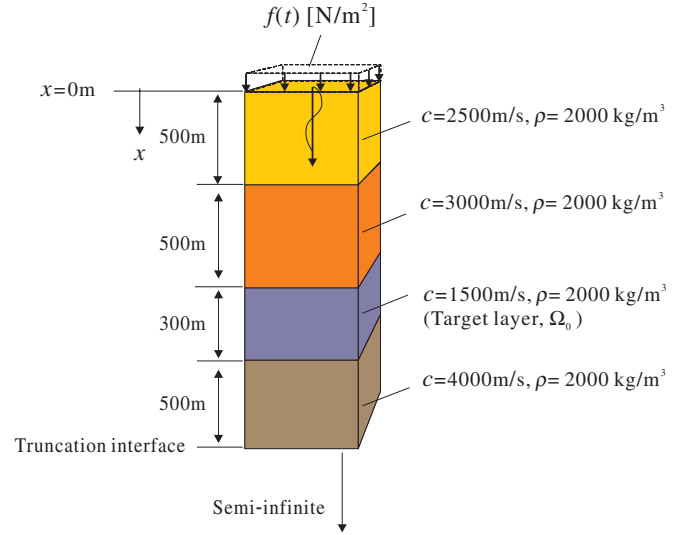


Figure 4. A four-layer heterogeneous domain; the truncation interface is located at the end of the fourth layer; the target layer is the softest of the formation (third layer).

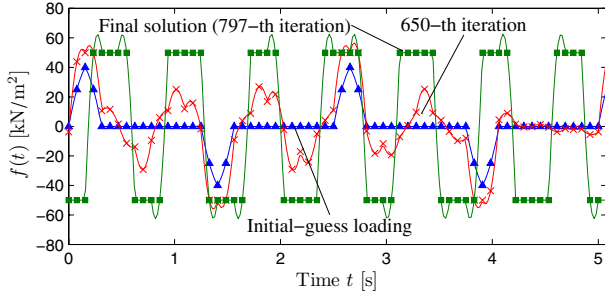
algorithm 1 Inversion algorithm

- 1: Set $\text{TOL} = 10^{-8}$, $\alpha = 0.9$ and $\beta = 1.1$
 - 2: Set $k = 0$ and initial force parameters $\mathbf{f}_{(0)}$
 - 3: Compute $\mathcal{L}_{(k)}$
 - 4: **while** ($e > \text{TOL}$) **do**
 - 5: Solve state problem (30a)
 - 6: Save state variables
 - 7: Solve adjoint problem (30b)
 - 8: Save adjoint variables
 - 9: Compute the search direction \mathbf{g} using CG
 - 10: **while** ($\mathcal{L}(\mathbf{f}_{(k)} + \theta_{(k)} \mathbf{g}) > \mathcal{L}(\mathbf{f}_{(k)} - \frac{1}{2} \theta_{(k)} \nabla \mathcal{L}(\mathbf{f}_{(k)}))$) **do**
 - 11: $\theta_{(k)} \leftarrow \alpha \theta_{(k)}$
 - 12: **end while**
 - 13: Update excitation parameters, $\mathbf{f}_{(k+1)}$ using (36)
 - 14: Compute $\mathcal{L}_{(k+1)}$
 - 15: Compute the iterative norm, e :

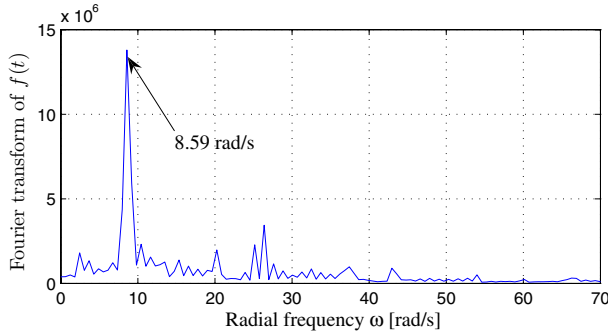
$$e = \frac{|\mathcal{L}_{(k+1)} - \mathcal{L}_{(k)}|}{|\mathcal{L}_{(k)}|}$$
 - 16: $\theta_{(k+1)} \leftarrow \beta \theta_{(k)}$
 - 17: $k \leftarrow k + 1$
 - 18: **end while**
-

5. Numerical results

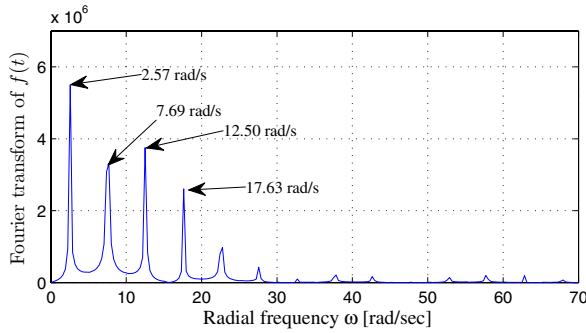
We report on numerical experiments to highlight the application of the outlined procedure. We consider a layered medium with four layers as depicted in figure 4. The loading is located on the surface ($x = 0$ m), and the truncation interface boundary is imposed at $x = 1800$ m. The layers are increasingly stiffer with depth, but are intercepted by a soft layer at 1000 m, which becomes the target layer. We use



(a) Iterative updates of the excitation $f(t)$ by minimizing (3); after 797 iterations, the initially-guessed perturbation loading converges to the final solution



(b) Frequency spectrum of the converged loading



(c) Frequency spectrum of the initial-guess loading

Figure 5. (a) Converged excitation form; (b) its Fourier transform; (c) the Fourier transform of the initial-guess loading.

linear isoparametric elements for the finite element solution of the state and adjoint problems with an element size of 10 m. The total observation time is set to $T = 20$ s, and the time step is 0.02 s. We use a periodic force function that has four periods within the T observation period. Each period is discretized using quadratic shape functions and 64 force nodes. We require that the nodal excitation parameter does not exceed 50 kN m^{-2} . The reduced gradient components are then evaluated as

$$\nabla_{f_i} \mathcal{L} = \int_0^T \lambda \sum_{j=1}^4 \varphi_{(i+64(j-1))}(t) dt \Big|_{x=0}. \quad (37)$$

We validated the derivation and implementation of the state, adjoint and control equations by comparing the values of the components of the gradient obtained using (37) to those of a numerically computed gradient obtained via a finite-difference method; both gradients were in excellent agreement.

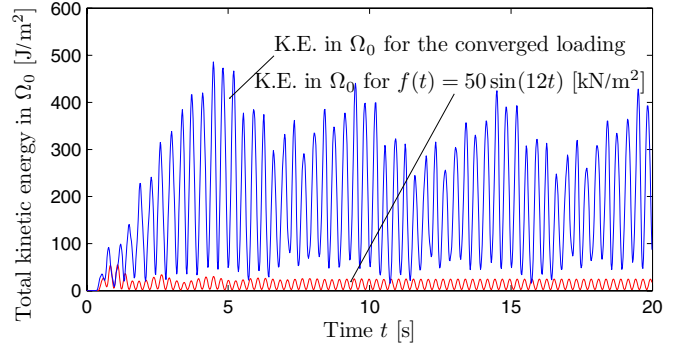


Figure 6. The kinetic energy in the target layer Ω_0 is much larger than that corresponding to a non-optimized loading.

5.1. Maximization of the kinetic energy in the target layer

First, we identify $f(t)$ that maximizes the kinetic energy in the target layer Ω_0 by minimizing the objective functional (3). To this end, we use the perturbation loading shown in figure 5 as the initial guess (shown with triangle symbols in the figure). The optimization process converges after 797 iterations to the near-periodic rectangular excitation shown also in figure 5; the dominant frequency of the converged loading is 8.59 rad s^{-1} (see the frequency spectrum of the converged loading shown in figure 5(b)).

We note that the optimization process resulted in the rendering of a complete time signal, including frequency content and amplitudes that differ significantly from those of the initial guess. For example, figure 5(c) depicts the Fourier transform of the initial guess, betraying a drastically different frequency content than that of figure 5(b). With respect to the amplitude, the peak value of the initial guess changed from 40 kN m^{-2} to about 50 kN m^{-2} for the converged loading. We remark that for all cases reported herein we use initial guesses with peak amplitudes below the capacity of modern-day Vibroseis equipment⁶.

Figure 6 shows that the total kinetic energy in the target layer Ω_0 for the converged optimized excitation is much larger than the kinetic energy for a non-optimized loading ($f(t) = 50 \sin(12t) \text{ kN m}^{-2}$). The amplitude of the non-optimized loading is set approximately equal to the dominant amplitude of the optimized loading. The total kinetic energy in Ω_0 is defined as $\int_{\Omega_0} K(x, t) d\Omega_0$, where the kinetic energy $K(x, t)$ is given by

$$K(x, t) = \frac{1}{2} \rho \left[\frac{\partial u(x, t)}{\partial t} \right]^2, \quad \text{in } \text{J m}^{-3}. \quad (38)$$

Next, we are concerned with kinetic energy measures both in the target layer Ω_0 and within its neighbours. Note that, as shown in figure 7(a), the kinetic energy distribution using the non-optimized source results in fairly low activity, when compared to the energy distribution shown in figure 7(b) that corresponds to the optimized source. Note further that, in this case, it is not only the target layer's energy that was affected, but also that of the layers lying above the target.

⁶ Modern Vibroseis sources could deliver up to 180 kN m^{-2} , and for frequencies up to 350 rad s^{-1} .

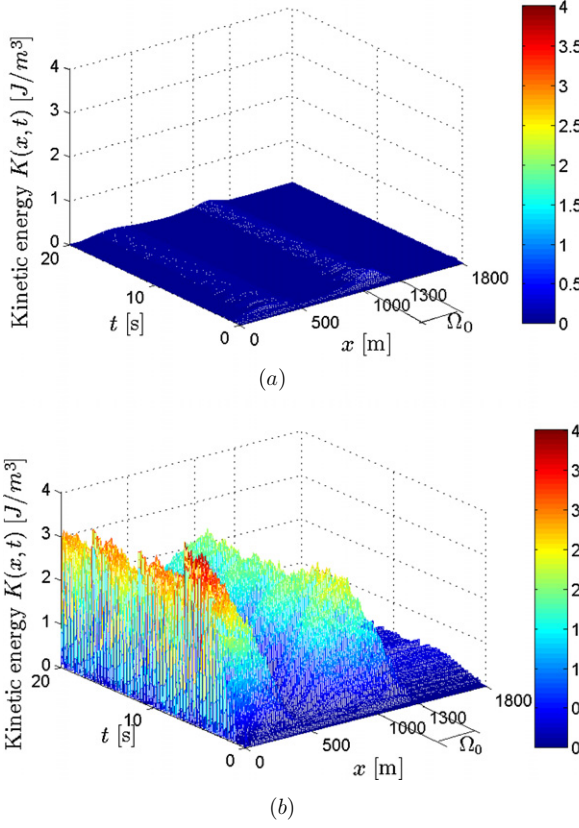


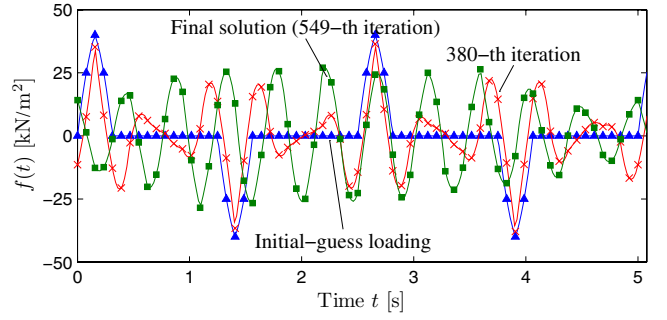
Figure 7. Distribution of the kinetic energy $K(x, t)$ using two different excitations. (a) Kinetic energy distribution over the entire domain using a suboptimal source ($f(t) = 50 \sin(12t) \text{ kN m}^{-2}$). (b) Kinetic energy distribution over the entire domain using the optimized source.

5.2. Selective energy focusing in the target layer—silent neighbours

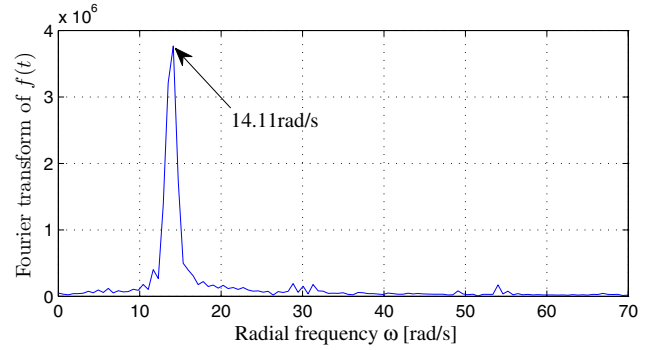
Next, we seek to identify $f(t)$ that maximizes the kinetic energy in the target layer Ω_0 using the objective functional (4), which aims at keeping the rest of the domain relatively inert. The excitation parameters converged after 549 iterations. As can be seen in figure 8(a), the finally converged loading appears to be sinusoidal of non-uniform amplitudes with a dominant frequency of 14.11 rad s^{-1} (the Fourier transform of the converged solution is shown in figure 8(b)).

Figure 9 shows that the inverted-for excitation selectively maximizes the distribution of kinetic energy in the target layer Ω_0 . By contrast, the kinetic energy distribution for a non-optimized loading signal, e.g. for $f(t) = 30 \sin(5t) \text{ kN m}^{-2}$, does not show the selective wave-energy focusing behaviour⁷. However, a monochromatic loading, $f(t) = 30 \sin(14.11t) \text{ kN m}^{-2}$, which uses the dominant frequency of the inverted-for loading also leads to the selective wave energy focusing in the target layer, while exhibiting stronger energy levels than the original inverted-for excitation. We conjecture that the optimization process converged to a local minimum,

⁷ We use the peak amplitude of the optimized loading (approximately 30 kN m^{-2}) as the amplitude for the non-optimized monochromatic loading.



(a) Iterative updates of the excitation $f(t)$ by minimizing (4); after 549 iterations, the initially-guessed perturbation loading converges to the final solution



(b) Frequency spectrum of the converged loading

Figure 8. (a) Converged excitation form, and (b) its Fourier transform.

within a larger basin of attraction around the 14.11 rad s^{-1} frequency.

Whereas the described process can successfully lead to excitations that could maximize the kinetic energy within a target layer, it is of interest to examine the level of motion induced by the converged signal in order to provide a preliminary assessment of its practicality. Figure 10 depicts the acceleration field within the target layer and at 1200 m from the surface. Figure 10(b) corresponds to the silent neighbouring layer case (maximum acceleration amplitude 0.2 m s^{-2}), whereas figure 10(a) corresponds to the case of the unconstrained layers (maximum acceleration amplitude 0.8 m s^{-2}). Even though such levels could lead to increased oil mobility (see the discussion in section 1), even higher levels are desirable. There are at least two ways we could use to investigate the possibility of inducing higher acceleration fields, while keeping the force amplitudes within the range of force that could be delivered by present-day equipment. Specifically, one could modify the objective functional to seek to maximize the acceleration field within the target layer instead of the kinetic energy. The functional would then be cast as

$$\mathcal{L} = \frac{1}{\int_{\Omega_0} \int_0^T \left[\frac{\partial^2 u}{\partial r^2}(x, t) \right]^2 dt dx}, \quad (39)$$

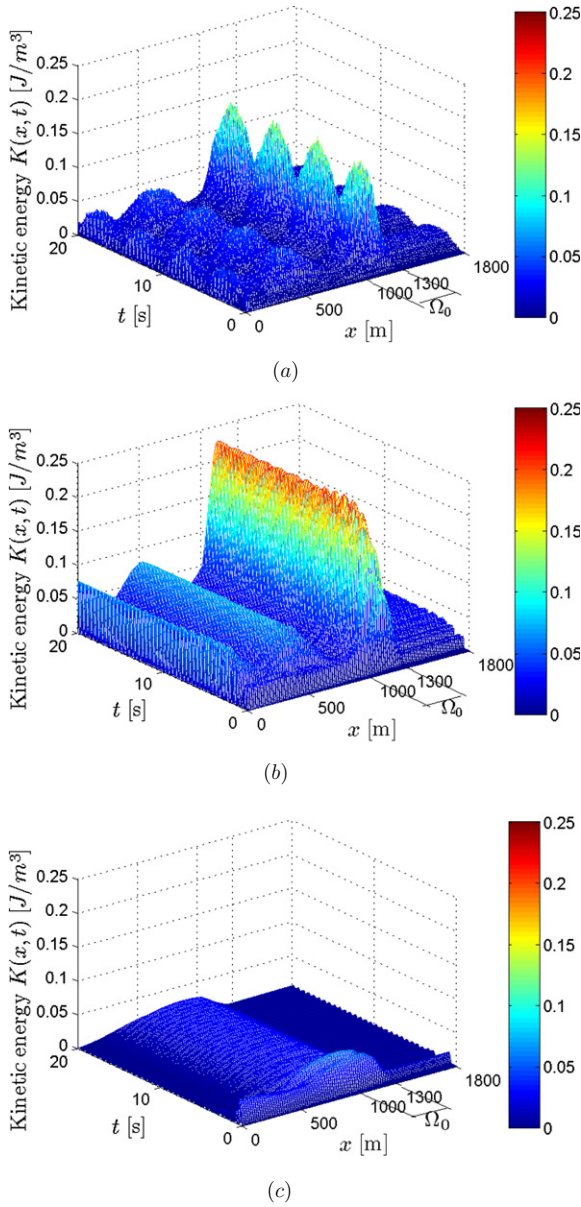


Figure 9. Distribution of the kinetic energy $K(x, t)$ for both optimized and non-optimized excitations. (a) Kinetic energy distribution for the converged excitation. (b) Kinetic energy distribution for $f(t) = 30 \sin(14.11t)$ kN m⁻² that uses the dominant frequency of the converged loading. (c) Kinetic energy distribution for a non-optimized source $f(t) = 30 \sin(5t)$ kN m⁻².

replacing (3) or, in the silent neighbours case, as

$$\mathcal{L} = \frac{\int_{\Omega \setminus \Omega_0} \int_0^T \left[\frac{\partial^2 u}{\partial t^2}(x, t) \right]^2 dt dx}{\int_{\Omega_0} \int_0^T \left[\frac{\partial^2 u}{\partial t^2}(x, t) \right]^2 dt dx}, \quad (40)$$

replacing (4). This will result in the following additional changes to the formulation.

- Equation (15) should be replaced by

$$\mathcal{E}(x) = \begin{cases} \frac{-2}{\left(\int_{\Omega_0} \int_0^T \left[\frac{\partial^2 u(x, t)}{\partial t^2} \right]^2 dt dx \right)^2}, & x \in \Omega_0, \\ 0, & x \in \Omega \setminus \Omega_0; \end{cases} \quad (41a)$$

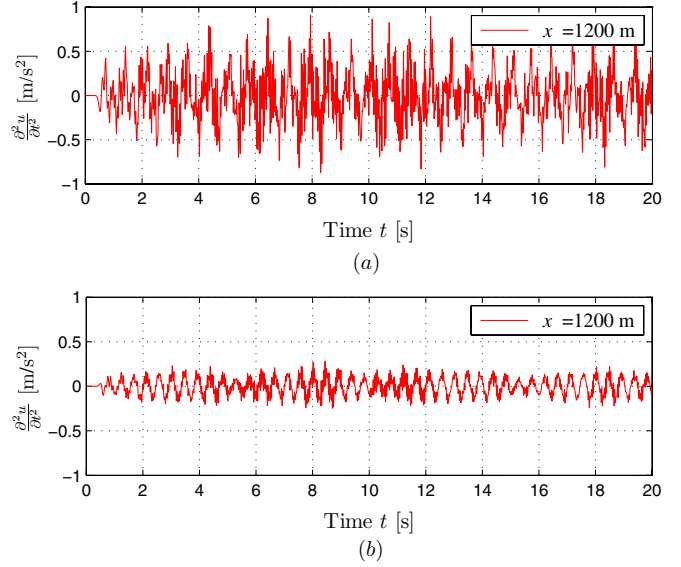


Figure 10. The acceleration in the target layer at $x = 1200$ m for the converged loadings. (a) The acceleration in the target layer for the converged excitation shown in figure 5(a). (b) The acceleration in the target layer for the converged excitation shown in figure 8(a).

- equation (18) should be replaced by

$$\mathcal{E}(x) = \begin{cases} \frac{-2 \int_{\Omega \setminus \Omega_0} \int_0^T \left[\frac{\partial^2 u(x, t)}{\partial t^2} \right]^2 dt dx}{\left(\int_{\Omega_0} \int_0^T \left[\frac{\partial^2 u(x, t)}{\partial t^2} \right]^2 dt dx \right)^2}, & x \in \Omega_0, \\ \frac{\int_{\Omega_0} \int_0^T \left[\frac{\partial^2 u(x, t)}{\partial t^2} \right]^2 dt dx}{\int_{\Omega_0} \int_0^T \left[\frac{\partial^2 u(x, t)}{\partial t^2} \right]^2 dt dx}, & x \in \Omega \setminus \Omega_0; \end{cases} \quad (41b)$$

- the adjoint problem (16) should be replaced by

$$\frac{\partial}{\partial x} \left(E \frac{\partial \lambda}{\partial x} \right) - \rho \frac{\partial^2 \lambda}{\partial t^2} = -\mathcal{E}(x) \frac{\partial^4 u}{\partial t^4}, \quad x \in (0, L), \quad t \in [0, T) \quad (41c)$$

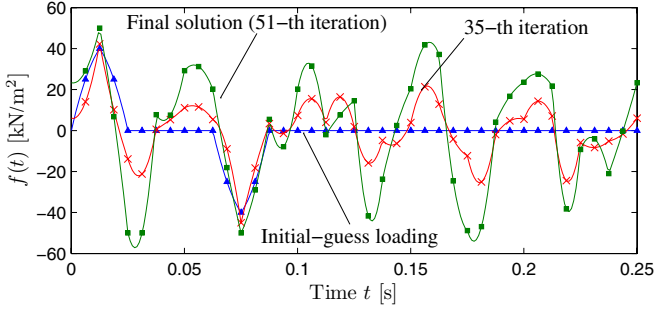
$$\frac{\partial \lambda}{\partial x}(0, t) = 0, \quad t \in [0, T) \quad (41d)$$

$$\frac{\partial \lambda}{\partial x}(L, t) - \frac{1}{c(L)} \frac{\partial \lambda}{\partial t}(L, t) = 0, \quad t \in [0, T) \quad (41e)$$

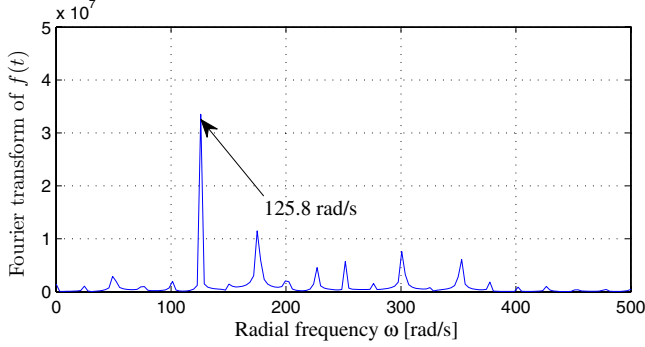
$$\lambda(x, T) = \frac{\mathcal{E}(x)}{\rho} \frac{\partial^2 u}{\partial t^2}(x, T), \quad x \in (0, L) \quad (41f)$$

$$\frac{\partial \lambda}{\partial t}(x, T) = \frac{\mathcal{E}(x)}{\rho} \frac{\partial^3 u}{\partial t^3}(x, T), \quad x \in (0, L). \quad (41g)$$

Alternatively, one could also use the maximization of the kinetic energy process with a finer discretization (in time) for the sought excitation signal, thereby allowing for higher driving frequencies. The number of elements used to discretize the signal (see equation (33)) controls, to an extent, the frequency content of the sought signal: a coarse time-discretization filters out high signal frequencies, since there are not enough points to capture them. By contrast, a finer discretization infuses flexibility, and allows for higher



(a) Iterative updates of the excitation $f(t)$ by minimizing (4)

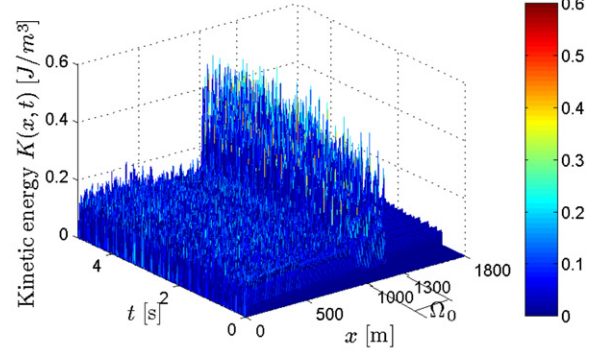


(b) Frequency spectrum of the converged loading

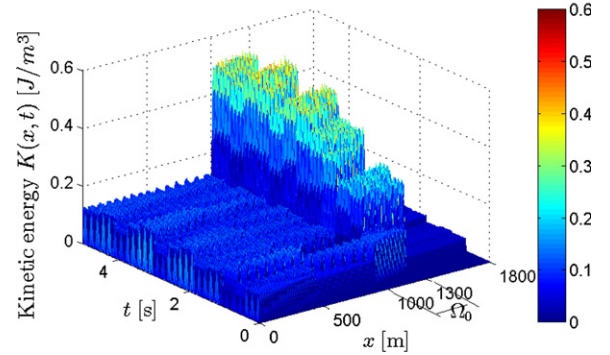
Figure 11. (a) Converged excitation form with the high frequency content, and (b) its Fourier transform.

frequency content. Using the same stratification as before, but a finer signal representation (the period of the time signal of the wave source is reduced to 0.25 s, and the total observation time is 5 s), we obtained the converged signal loading shown in figure 11, with a time step of 0.001 s. Note that the Fourier transform of the signal reveals now a higher dominant frequency than before (figure 11(b)), i.e. 125.8 rad s^{-1} versus 14.11 rad s^{-1} . Using an amplitude of 50 kN m^{-2} (peak amplitude of an optimized signal), the kinetic energies for the inverted-for signal as well as its monochromatic counterpart are shown in figure 12. Moreover, figure 13 depicts the acceleration field within the target layer and at 1200 m, which shows an amplitude of about 4.0 m s^{-2} . The acceleration field is now significant, and is within the range that could increase oil mobility (Beresnev 2006).

The entire process, as described herein, was based on one-dimensional assumptions. As mentioned, it is impossible to replicate in the field one-dimensional conditions, for, even if the underlying stratification were layered, the excitation would have to be uniformly distributed over a fairly large surface to induce truly one-dimensional behaviour. We used a maximum amplitude of 50 kN m^{-2} , which is difficult to replicate with even a fleet of Vibroseis sources spread over the ground surface, even though each Vibroseis could deliver 180 kN m^{-2} , almost four times the amplitudes we used herein. However, what has not been taken into account in this one-dimensional analysis is the potentially beneficial constructive wave energy interference an optimal distribution of the sources could achieve for given site conditions, which could, in turn, result in the multi-fold increase of the accelerations. Thus far,



(a)



(b)

Figure 12. Distribution of the kinetic energy $K(x, t)$ for the optimal excitations with a high-frequency content. (a) Kinetic energy distribution for the converged excitation shown in figure 11. (b) Kinetic energy distribution for $f(t) = 50 \sin(125.8t) \text{ kN m}^{-2}$ that uses the dominant frequency of the converged loading shown in figure 11.

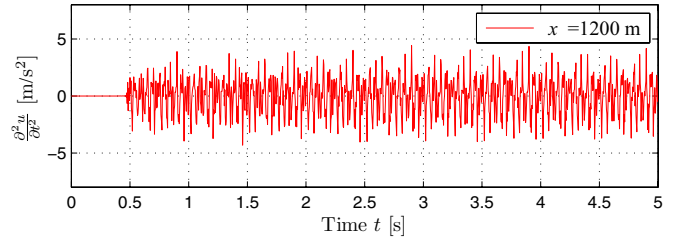


Figure 13. The acceleration in the target layer for the converged excitation shown in figure 11.

we have shown that the outlined optimization process can lead to arbitrary excitation signals, which contain strong single-frequency components. It is of interest to study the relation of the optimized signal's frequencies to the exact frequencies necessary for maximizing the kinetic energy in the target layer, in order to assess the optimizer's performance. The one-dimensional nature of the prototype problem lends itself easily to the exact solution. We remark that since the problem involves a domain of semi-infinite extent, there are no resonant frequencies in the classic sense. However, there is a set of frequencies for which the response is amplified compared to others: for the remainder, we term these frequencies, amplification frequencies. To obtain them, we study the frequency dependence of the wave response in the prototype

four-layered system shown in figure 4 by considering the time-harmonic response within each layer:

$$\begin{aligned}
 u_1(x, t) &= [A_{11} \exp(-ik_1x) + A_{12} \exp(ik_1x)] \exp(i\omega t), \\
 0 &= x_1 \leq x < x_2, \\
 u_2(x, t) &= [A_{21} \exp(-ik_2x) + A_{22} \exp(ik_2x)] \exp(i\omega t), \\
 x_2 &\leq x < x_3, \\
 u_3(x, t) &= [A_{31} \exp(-ik_3x) + A_{32} \exp(ik_3x)] \exp(i\omega t), \\
 x_3 &\leq x < x_4, \\
 u_4(x, t) &= [A_{41} \exp(-ik_4x)] \exp(i\omega t), \quad x_4 \leq x, \quad (42)
 \end{aligned}$$

where ω denotes the radial frequency of the wave motions; $k_n = \omega/c_n$ denotes the wavenumber in the n th layer and c_n denotes the wave speed in the n th layer. With the time harmonic factor $\exp(i\omega t)$, $A_{n1} \exp(-ik_nx)$ and $A_{n2} \exp(ik_nx)$ represent the outgoing and reflected waves in the n th layer with amplitudes A_{n1} and A_{n2} , respectively. In addition, on the surface ($x = 0$), there holds

$$E_1 \frac{\partial u_1(x, t)}{\partial x} = P \exp(i\omega t). \quad (43)$$

The following continuity conditions also hold:

$$\begin{aligned}
 u_1(x_2, t) &= u_2(x_2, t), \quad E_1 \frac{\partial u_1(x_2, t)}{\partial x} = E_2 \frac{\partial u_2(x_2, t)}{\partial x}, \\
 u_2(x_3, t) &= u_3(x_3, t), \quad E_2 \frac{\partial u_2(x_3, t)}{\partial x} = E_3 \frac{\partial u_3(x_3, t)}{\partial x}, \quad (44) \\
 u_3(x_4, t) &= u_4(x_4, t), \quad E_3 \frac{\partial u_3(x_4, t)}{\partial x} = E_4 \frac{\partial u_4(x_4, t)}{\partial x}.
 \end{aligned}$$

Therefore, (42)–(44) give rise to the following system of equations:

$$\begin{bmatrix}
 -E_1 ik_1, E_1 ik_1, 0, 0, 0, 0 \\
 e^{-ik_1x_2}, e^{ik_1x_2}, -e^{-ik_2x_2}, -e^{ik_2x_2}, 0, 0, 0 \\
 -E_1 ik_1 e^{-ik_1x_2}, E_1 ik_1 e^{ik_1x_2}, E_2 ik_2 e^{-ik_2x_2}, -E_2 ik_2 e^{ik_2x_2}, 0, 0, 0 \\
 0, 0, e^{-ik_2x_3}, e^{ik_2x_3}, -e^{-ik_3x_3}, -e^{ik_3x_3}, 0 \\
 0, 0, -E_2 ik_2 e^{-ik_2x_3}, E_2 ik_2 e^{ik_2x_3}, E_3 ik_3 e^{-ik_3x_3}, -E_3 ik_3 e^{ik_3x_3}, 0 \\
 0, 0, 0, 0, e^{-ik_3x_4}, e^{ik_3x_4}, -e^{-ik_4x_4} \\
 0, 0, 0, 0, -E_3 ik_3 e^{-ik_3x_4}, E_3 ik_3 e^{ik_3x_4}, E_4 ik_4 e^{-ik_4x_4}
 \end{bmatrix}
 \times
 \begin{bmatrix}
 A_{11} \\
 A_{12} \\
 A_{21} \\
 A_{22} \\
 A_{31} \\
 A_{32} \\
 A_{41}
 \end{bmatrix}
 =
 \begin{bmatrix}
 P \\
 0 \\
 0 \\
 0 \\
 0 \\
 0 \\
 0
 \end{bmatrix}. \quad (45)$$

Solving for the coefficients A_{11}, \dots, A_{41} in (45) leads to the solution for the total wave fields in (42) (there are no roots to the determinant). For example, for the given stratification shown in figure 4 and for a force amplitude of $P = 50 \text{ kN m}^{-2}$, the time-harmonic response solution $u_3(x, t)$ in the target layer becomes

$$\begin{aligned}
 u_3(x, t) &= \frac{\left(\frac{22}{5} i e^{-\frac{i\omega(-1300+x)}{1500}} - 2 i e^{\frac{i\omega(-1300+x)}{1500}} \right) e^{i\omega t}}{\omega \left(165 e^{-\frac{17}{30} i\omega} - 5 e^{-\frac{7}{30} i\omega} - 11 e^{\frac{7}{30} i\omega} - 22 e^{\frac{i\omega}{6}} + 363 e^{\frac{17}{30} i\omega} - 106 e^{-\frac{i\omega}{6}} \right)}. \quad (46)
 \end{aligned}$$

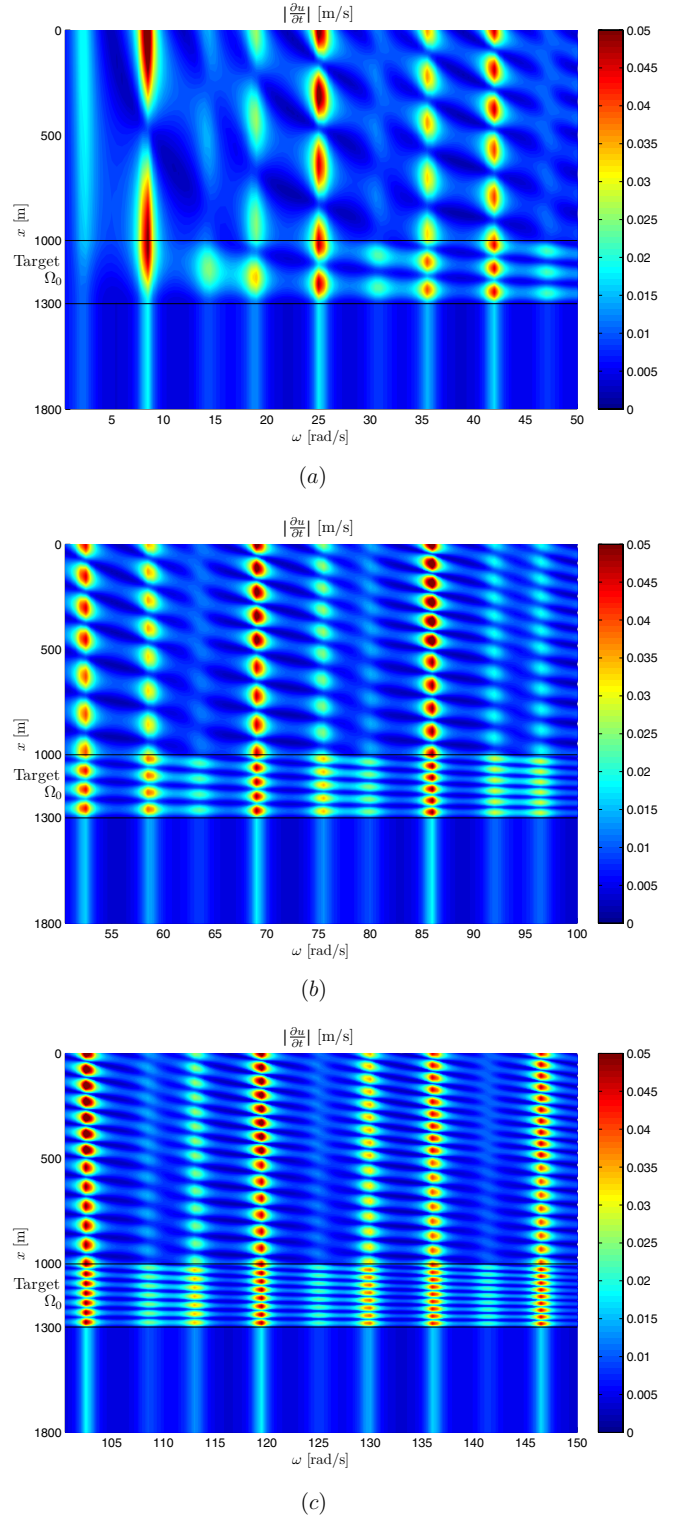


Figure 14. Frequency sweep of the particle velocity $|\frac{\partial u}{\partial t}|$ within the truncated semi-infinite layered system: (a) $\omega = 0\text{--}50 \text{ rad s}^{-1}$, (b) $\omega = 50\text{--}100 \text{ rad s}^{-1}$ and (c) $\omega = 100\text{--}150 \text{ rad s}^{-1}$.

Clearly, (46) has no resonant frequencies for $\omega \neq 0$. The same applies to the motion within the other layers. However, there are frequencies for which the motion is amplified. Figure 14 depicts the distribution of the amplitude of the

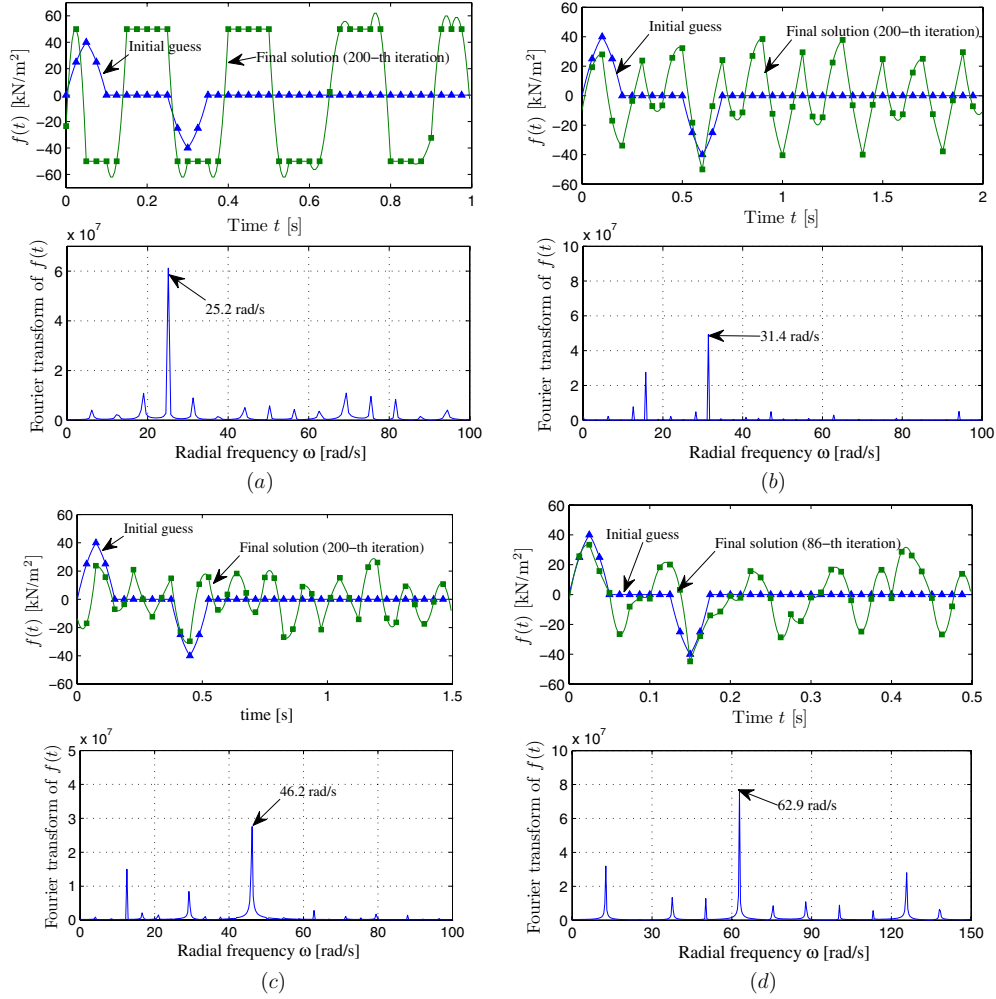


Figure 15. Inverted-for signals showing strong components at the theoretically exact amplification frequencies. (a) The optimized time signal after the minimization of \mathcal{L}_1 (all layers are active) with a loading period of 1 s. (b) The optimized time signal after the minimization of \mathcal{L}_2 (silent neighbours) with a loading period of 2 s. (c) The optimized time signal after the minimization of \mathcal{L}_2 (silent neighbours) with a loading period of 1.5 s. (d) The optimized time signal after the minimization of \mathcal{L}_2 (silent neighbours) with a loading period of 0.5 s.

particle velocity $\left| \frac{\partial u}{\partial t} \right|$ of the time-harmonic motion with respect to space, and for a frequency sweep between 0 and 150 rad s^{-1} . Note that at discrete frequencies close to 8.4 rad s^{-1} , 25.2 rad s^{-1} , 41.9 rad s^{-1} , etc there is strong motion amplification in *all* layers, not just the target. By contrast, at frequencies close to 14.2 , 30.7 , 47.1 , \dots , 125 rad s^{-1} , etc motion amplification is only observed in the target layer. As shown earlier, the optimization process we described recovered effectively signals exhibiting strong components at these amplification frequencies: for example, figure 5 shows motion amplification at 8.59 rad s^{-1} (versus 8.4 rad s^{-1}), whereas figure 8 shows 14.11 rad s^{-1} (versus 14.2 rad s^{-1} ; silent neighbours), and figure 11 shows the motion amplification at 125.8 rad s^{-1} . For completeness, we remark that by simply changing the loading period the optimizer would reconstruct loading signals exhibiting strong components at other amplification frequencies, as can be seen in figure 15. Thus, we would conjecture that the optimization scheme is a very effective agent for computing monochromatic excitation signals aimed at maximizing a desired metric in a target formation.

6. Discussion

We described a systematic process that allows the determination of an unknown excitation when seeking to maximize mobility in a targeted formation embedded within a heterogeneous domain. We cast the problem as an inverse-source problem, and used a partial-differential-equation-constrained optimization scheme to arrive at a triplet of state, adjoint and control problems. Solving the problem triplet yields an excitation, which over many others, would result in large kinetic energy distributions within the target formation. Since there is no guarantee of convexity of the augmented objective functional, nor a guarantee that the process would yield the global maximum, the procedure can be viewed as a vehicle for avoiding the blind prescription of excitations: one should be mindful that another excitation may exist that could yield the global maximum.

Numerical results show that there certainly exists an optimal time signal of the loading function that can maximize the wave energy in the target layer. The kinetic energy in the target layer for the converged optimized source signal is

several times larger than the kinetic energy for a non-optimized source signal. The optimizer also identifies a loading signal that can selectively maximize the kinetic energy in the target layer, while the kinetic energy in the neighbouring layers is minimized. The inversion process resulted in excitations that are well within the specification of present-day equipment, and capable of inducing significant acceleration fields, which, in turn, could mobilize oil in existing reservoirs.

The procedure, nearly unaltered, could be extended to the all-important three-dimensional elastic wave case; it is well suited for wave-based EOR applications, when given a known formation and a target reservoir. Though the focus here was on maximizing kinetic energy, other maximization targets could be equally well accommodated (we have also discussed the maximization of the acceleration field). The extensions to the two- and three-dimensional cases will be communicated in the future.

Acknowledgments

This work was partially supported by an Academic Excellence Alliance grant with KAUST, the King Abdullah University of Science and Technology and by the Department of Petroleum and Geosystems Engineering of the University of Texas at Austin. This support is gratefully acknowledged.

References

- Beresnev I A 2006 Theory of vibratory mobilization on nonwetting fluids entrapped in pore constrictions *Geophysics* **71** 47–56
- Beresnev I A and Johnson P 1994 Elastic-wave stimulation of oil production: a review of methods and results *Geophysics* **59** 1000–17
- Fletcher R and Reeves C M 1951 Function minimization by conjugate gradients *Comput. J.* **7** 149–54
- Guo X, Du Z, Li G and Shu Z 2004 High frequency vibration recovery enhancement technology in the heavy oil fields of China *Proc. SPE Int. Thermal Operations and Heavy Oil Symp. and Western Regional Meeting (Bakersfield, CA)* SPE 86956
- Huh C 2006 Improved oil recovery by seismic vibration: a preliminary assessment of possible mechanisms *Proc. 1st Int. Petrol. Conf. (Cancun, Mexico)* SPE 103870
- Iassonov P P and Beresnev I A 2003 A model for enhanced fluid percolation in porous media by application of low-frequency elastic waves *J. Geophys. Res.* **108** 2138–46
- Karush W 1939 Minima of functions of several variables with inequalities as side constraints *Master Thesis* University of Chicago
- Kouznetsov O L, Simkin E M, Chilingar G V and Katz S A 1998 Improved oil recovery by application of vibro-energy to waterflooded sandstones *J. Petrol. Sci. Eng.* **19** 191–200
- Kuhn H W and Tucker A W 1951 *Nonlinear programming 2nd Berkeley Symposium on Mathematical Statistics and Probability* (Berkeley, CA: University of California Press)
- Kuznetsov O L, Simkin E M, Chilingar G V, Gorfunkel M V and Robertson J O 2002 Seismic techniques of enhanced oil recovery: experimental and field results *Energy Sources* **24** 877–89
- Kuznetsov V V and Nikolaev A V 1990 Elaboration of physical principles of vibro-seismic action on oil reservoir (Razrabotka fizicheskikh osnov vibroseismicheskogo vozdeystviya na nefitanyouyou zalezh) *Report* Institute of Physics of the Earth, Moscow, Russia (in Russian)
- Lake L W 1989 *Enhanced Oil Recovery* (Englewood Cliffs, NJ: Prentice-Hall)
- Li W, Vigil R D, Beresnev I A, Iassonov P P and Ewing R 2005 Vibration-induced mobilization of trapped oil ganglia in porous media: experimental validation of a capillary-physics mechanism *J. Colloid Interface Sci.* **289** 193–9
- Nocedal J and Wright S 2006 *Numerical Optimization* (New York: Springer)
- Osika D G 1981 *Fluid Regime of Seismically Active Regions (Fluidniy Rejim Seismicheskoi-aktivnikh Oblastey)* (Moscow: Nauka)
- Smimova M N 1968 Effect of earthquakes on the oil yield of the Gudermes field (Northeastern Caucasus) *Physics of the Solid Earth (Fizika Zemli)* vol 12 (USSR: Izvestiya Academy of Sciences) pp 71–6
- Steinbrugge K V and Moran D F 1954 An engineering study of the Southern California earthquake of July 21, 1952, and its aftershocks *Bull. Seismol. Soc. Am.* **44** 279–83
- Surguchev L, Koundin A, Melberg O, Rolfsvåg T and Menard W P 2002 Cyclic water injection: improved oil recovery at zero cost *Pet. Geosci.* **8** 89–95
- Voytov G I, Osika D G, Grechukhina T G and Plotnikov I A 1972 Some geological and geochemical consequences of the Dagestan earthquake of May 14, 1970 *Trans. USSR Acad. Sci., Earth Sci. Sections* **202** 576–9 (in Russian)
- Westermarck R V, Brett J F and Maloney D R 2001 Using downhole vibration stimulation for enhanced oil recovery *World Oil* 57–66
- Zhu T and Xutao H 2005 Downhole harmonic vibration oil-displacement system: a new IOR tool *Proc. SPE Western Regional Meeting (Irvine, CA)* SPE 94001-MS